



La Science à l'œuvre pour le  
at work for Canada

## NRC Publications Archive (NPArc) Archives des publications du CNRC (NPArc)

### **Effects of the Fractal Prefactor on the Optical Properties of Fractal Soot Aggregates**

Liu, Fengshan; Snelling, David R.; Smallwood, Gregory J.

#### **Publisher's version / la version de l'éditeur:**

*Proceedings of ASME 2009 2nd Micro/Nanoscale Heat & Mass Transfer (MNHMT 2009) International Conference, 2009., 2009-12-22*

#### **Web page / page Web**

<http://nparc.cisti-icist.nrc-cnrc.gc.ca/npsi/ctrl?action=rtdoc&an=15473823&lang=en>  
<http://nparc.cisti-icist.nrc-cnrc.gc.ca/npsi/ctrl?action=rtdoc&an=15473823&lang=fr>

Access and use of this website and the material on it are subject to the Terms and Conditions set forth at

[http://nparc.cisti-icist.nrc-cnrc.gc.ca/npsi/jsp/nparc\\_cp.jsp?lang=en](http://nparc.cisti-icist.nrc-cnrc.gc.ca/npsi/jsp/nparc_cp.jsp?lang=en)

READ THESE TERMS AND CONDITIONS CAREFULLY BEFORE USING THIS WEBSITE.

L'accès à ce site Web et l'utilisation de son contenu sont assujettis aux conditions présentées dans le site

[http://nparc.cisti-icist.nrc-cnrc.gc.ca/npsi/jsp/nparc\\_cp.jsp?lang=fr](http://nparc.cisti-icist.nrc-cnrc.gc.ca/npsi/jsp/nparc_cp.jsp?lang=fr)

LISEZ CES CONDITIONS ATTENTIVEMENT AVANT D'UTILISER CE SITE WEB.

Contact us / Contactez nous: [nparc.cisti@nrc-cnrc.gc.ca](mailto:nparc.cisti@nrc-cnrc.gc.ca).



National Research  
Council Canada

Conseil national  
de recherches Canada

Canada

**MNHMT2009-18473**

## **Effects of the Fractal Prefactor on the Optical Properties of Fractal Soot Aggregates**

**Fengshan LIU, David R. SNELLING, Gregory J. SMALLWOOD**

Institute for Chemical Process and Environmental Technology, National Research Council  
Building M-9, 1200 Montreal Road, Ottawa, Ontario, Canada K1A 0R6

### **ABSTRACT**

The effects of prefactor on the optical properties of numerically generated fractal soot aggregates were investigated using the numerically exact generalized multi-sphere Mie-solution method (GMM) and the approximate Rayleigh-Debye-Gans (RDG) theory. The numerically generated fractal aggregates consist of 50 to 400 primary particles of 30 nm in diameter. The considered incident laser wavelength is 266 nm. Attention is paid to the effect of prefactor on the vertical-vertical differential scattering cross section, since such quantity has often been used to infer the fractal dimension and prefactor based on the RDG formulation. The fractal prefactor affects the optical properties of the numerically generated soot aggregates through its influence on the compactness of the structure. Using GMM to calculate the optical properties of the numerically generated aggregates results in a lower aggregate absorption cross section, but a higher total scattering cross section with increasing the prefactor. The difference between the RDG results and those of GMM is primarily caused by multiple scattering and such effect is found significant, especially for the higher value of prefactor considered. The fractal dimension derived from the GMM non-dimensional differential scattering cross section agrees well with the morphological value in the case of the lower prefactor of 1.3 considered; however, the derived fractal dimension is much higher than the morphological value for fractal soot aggregates with a prefactor of 2.3. The light scattering derived prefactor is in general lower than the morphological value, especially when the morphological prefactor is higher.

**Keywords:** Light scattering, Fractal aggregate, Multiple Scattering, RDG Approximation, Generalized Mie-solution

### **INTRODUCTION**

Aggregates consisting of nano-sized small spherical particles (hereafter called primary particles) are produced in many practical applications, such as soot aggregates from engines and combustors. The formation of aggregates is a result of particle aggregation. These aggregates can often be considered as mass fractals whose structure can be described by the statistical scaling law (see Eq. 1 below), namely the radius of gyration is related to the primary particle radius, the number of primary particles in the aggregate (hereafter termed the aggregate size), the fractal dimension and the fractal prefactor. The optical properties of fractal aggregates are of great interest and importance for various reasons, such as for accurate calculations of thermal radiative transfer in sooting flames and accurate measurements of particle concentration and morphology using optical diagnostics. For combustion generated soot measurements, the conventional techniques include light extinction and soot thermal emission in the visible and near infrared. The more recently developed approaches include the laser-induced incandescence (LII), laser scattering (LS), or a combination of LII/LS. The accuracy of these techniques is largely determined by our knowledge of the optical properties of fractal soot aggregates.

Owing to the complex structure of fractal aggregates their optical properties cannot be described by the classical Mie theory for spherical particles [1,2], but can be reasonably predicted by the relatively simple Rayleigh-Debye-Gans (RDG) approximation [3,4]. The RDG approximation has been commonly used to interpret the experimental results in LS experiments to infer the morphological parameters of soot and other fractal aggregates. The validity of the RDG approximation has been investigated in several studies, e.g.

[4,5], and these numerical simulations suggest that the RDG approximation, which neglects the multiple scattering within the aggregate, underestimates the aggregate absorption cross section by up to about 15% and can also lead to poor accuracy for the aggregate scattering properties under certain conditions such as large primary particle size parameter and aggregate size.

Besides the primary particle radius and the aggregate size, the radius of gyration of the aggregate depends on both the fractal dimension and the fractal prefactor. Compared to the fractal dimension, the fractal prefactor has received less attention [6]. It is worth pointing out that for a given aggregate size the compactness of the aggregates is dependent on both the fractal dimension and the prefactor in such a way that an increase in the value of either of these two parameters results in a more compact structure, although the effect of fractal dimension is much stronger, especially for very large aggregates. Therefore, the optical properties of fractal aggregates are dependent on both the fractal dimension and the prefactor. The latter is the concern of the present study.

One of the important results of the RDG approximation for the optical properties of fractal aggregates is that the fractal dimension can be recovered from the slope of the non-dimensional differential scattering cross section in the power-law regime when plotted against the non-dimensional modulus of the scattering vector on a log-log scale [6,7]. This result has been commonly used to infer the fractal dimension of soot aggregates experimentally using the LS technique, e.g. [7]. However, it was shown by Brasil et al. [6] that the numerically predicted scattering properties of numerically generated monodisperse fractal aggregates of known fractal dimension and prefactor in general do not recover the expected morphological fractal dimension and prefactor. In their study, the optical properties of fractal aggregates were calculated using the integral equations formulation for scattering (IEFS), which accounts for multiple scattering among primary particles and is believed to be reasonably accurate for primary particle size parameters up to 0.4 [6]. It was shown by Brasil et al. [6] that the fractal dimension recovered from the slope of the non-dimensional differential scattering cross section in the power-law regime is in general different from the morphological fractal dimension. Although the study of Brasil et al. [6] suffers the drawbacks that there are variations in the morphological fractal dimension and prefactor among the aggregates investigated and insufficient orientations (only 16) were used to conduct orientation averaging, the disagreement revealed in their study between the fractal dimension recovered from the predicted differential scattering cross section and the morphological one can indeed be expected from the fact that multiple scattering is accounted for in the IEFS calculations, but absent from the RDG approximation, which serves the basis for recovering the fractal dimension from the slope of the differential scattering cross section in the power-law regime. The study of Brasil et al. [6] also made an attempt to highlight the importance of fractal prefactor.

The present study was motivated by the lack of adequate understanding of the effect of multiple scattering on the slope of the non-dimensional differential scattering cross section in the power-law regime on a log-log scale. In particular, the effects of the fractal prefactor on the optical properties of fractal aggregates and on the extent of multiple scattering were investigated numerically. The objective of this study is to gain an improved understanding of the contribution of multiple scattering to the discrepancy between the morphological fractal dimension and that inferred from the slope of the non-dimensional differential scattering cross section in the power-law regime.

## METHODOLOGY

### Numerically Generated Fractal Aggregates

For the purpose of the present numerical study, fractal aggregates of identical fractal dimension but different prefactors need to be generated. Soot, like many other fractal objects, is formed by the aggregation of small, nearly identical and spherical primary particles into complex geometries. This assumption (primary particles are uniform and identical spheres) has been commonly made in almost all previous numerical studies and it was also made here. The fractal-like structure of such aggregates obey the following statistical scaling law [8]

$$N = k_f \left( \frac{R_g}{a} \right)^{D_f} \quad (1)$$

where  $N$  is the number of primary particles within the aggregate (aggregate size),  $k_f$  and  $D_f$  are the prefactor and fractal dimension, respectively,  $a$  is the primary particle radius, and  $R_g$  is the radius of gyration defined as [9]

$$R_g^2 = \frac{1}{N} \sum_{i=1}^N (\mathbf{r}_i - \mathbf{r}^0)^2 + a^2 \quad (2)$$

$$\mathbf{r}^0 = \frac{1}{N} \sum_{i=1}^N \mathbf{r}_i \quad (3)$$

where vectors  $\mathbf{r}_i$  and  $\mathbf{r}^0$  define the position of the centre of  $i$ th primary particle and the centre of the aggregate, respectively. In this study, fractal aggregates with prescribed values of  $D_f$  and  $k_f$  were numerically generated using the particle-cluster aggregation algorithm for small aggregates (up to  $N = 31$ ) and cluster-cluster aggregation algorithm for larger aggregates. The algorithms follow closely those described by Filippov et al. [9] and the details of our numerical implementation of these algorithms can be found in [5]. Compared to some other algorithms based on mimicking the physical processes of aggregate formation, such as [6,10], which generate aggregates with a certain variation in the fractal dimension and/or the fractal prefactor, the method used here offers the advantage that there is excellent consistency in the fractal parameters ( $D_f$  and  $k_f$ ) among the numerically generated aggregates, since Eq. (1) is strictly satisfied under specified values of  $D_f$  and  $k_f$ . As a result, the fractal aggregates generated using the present method are suitable for investigating the effect of either  $D_f$  or  $k_f$

on the optical or other properties (such as thermal) of fractal aggregates.

The following morphological parameters were used in the generation of all fractal aggregates:  $D_f = 1.78$ ,  $a = 15$  nm, which are typical values for flame-generated soot. Two different values of the prefactor,  $k_f = 1.3$  and  $2.3$ , were used to generate aggregates of different compactness. Fractal aggregates consisting of  $N = 50, 100, 200$ , and  $400$  primary particles were generated for both prefactors. It is noticed that for a given set of morphological parameters ( $a$ ,  $N$ ,  $D_f$ , and  $k_f$ ) there are endless possibilities in the arrangement of individual primary particles. It has been shown in previous studies, e.g. [11], that it is important to perform configuration averaging, in addition to orientation averaging, to achieve more accurate optical properties of a random-oriented ensemble of monodisperse aggregates. In this study, at least 10 different realizations were generated for a given set of morphological parameters.

To demonstrate the effect of the prefactor on the compactness of the fractal structure and the variability in the arrangement of primary particles in aggregates of identical morphology, several typical aggregate configurations for  $N = 100$  are displayed in Fig. 1. It is evident that the aggregates can have very different arrangements of individual primary particles for identical morphological parameters of  $a$ ,  $N$ ,  $D_f$ , and  $k_f$ , compare Figs. 1(a)-1(c) or Figs. 1(d)-1(f). The overall structure of the aggregates becomes more compact as  $k_f$  increases, compare the bottom row figures to the top row ones. It is expected that both the primary particle size parameter and the compactness of the fractal structure affect the importance of multiple scattering.

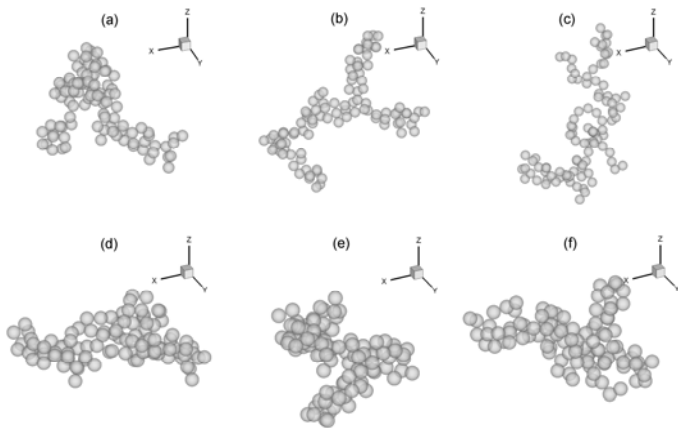


Fig. 1 Typical fractal aggregates consisting of  $N = 100$  primary particles of  $d_p = 30$  nm with  $D_f = 1.78$ . For (a)-(c)  $k_f = 1.3$ . For (d)-(f)  $k_f = 2.3$

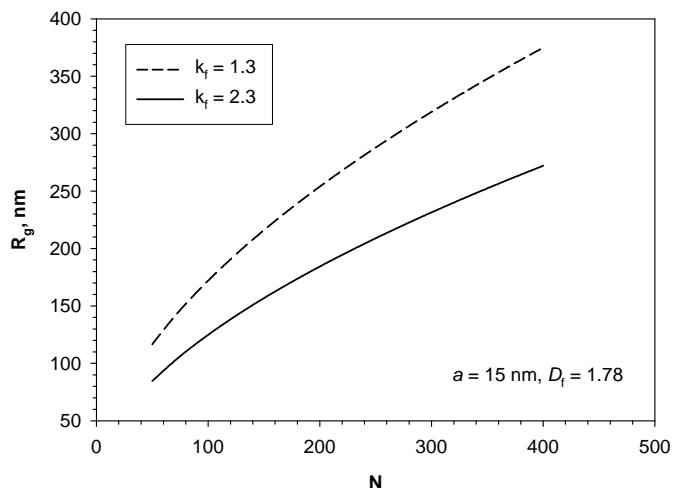


Fig. 2 Variation of the radius of gyration with aggregate size  $N$  for two different values of  $k_f$

The effect of the prefactor on the overall appearance or compactness of an aggregate can also be revealed by examining the variation of the radius of gyration with  $k_f$  from Eq. (1). Fig. 2 compares the radii of gyration of different aggregate sizes for  $k_f = 1.3$  and  $2.3$ . It is clear that  $k_f$  affects significantly the radius of gyration in such a way that it becomes much smaller as  $k_f$  increases, especially for large aggregates. A smaller radius of gyration for given  $a$  and  $N$  implies that the structure is more compact.

Besides the statistical scaling relationship, Eq. (1), it is also expected that the density autocorrelation function of fractal aggregates have the following functional form [12]

$$C(r) = Ar^{D_f-3}h(r/\xi) \quad (4)$$

where  $C(r)$  is the density autocorrelation or two-point density-density correlation function,  $r$  is the distance variable,  $A$  is an appropriate constant,  $h$  is a cutoff function associated with the finite size of aggregates, and  $\xi$  is a characteristic length representing the size of the aggregate. Eq. (4) implies that the autocorrelation function  $C(r)$ , when plotted on a log-log scale, should display a slope of  $(D_f-3)$  over an intermediate range of  $r$ . It is noticed that although the scaling law, Eq.(1), is satisfied by all the numerically generated fractal aggregates, there is no guarantee that the autocorrelation functions of these aggregates have the correct slope. Therefore, it is important to check this aspect of the numerically generated aggregates before their optical properties are calculated, since it is well known that the autocorrelation function is directly linked to the scattering behavior of fractal aggregates [9,12].

The autocorrelation function was calculated as the distance distribution function described by Hasmy et al. [13] and Filippov et al. [9]. Some typical results of  $C(r)$  vs. the non-dimensional distance  $r/d_p$  are shown in Fig. 3. These results are averaged over 10 aggregate realizations of identical parameters. Two observations can be made from Fig. 3. First, all curves display the correct slope at an intermediate range of  $r/d_p$ ,

though it is more evident for larger  $N$ . Secondly, the autocorrelation functions for  $k_f = 1.3$  are lower at small distances but higher at larger ones. This is expected since their structures are more open as shown in Figs. 1 and 2. The results shown in Fig. 3 confirm that the numerically generated fractal aggregates indeed satisfy the fractal property given in Eq. (4).

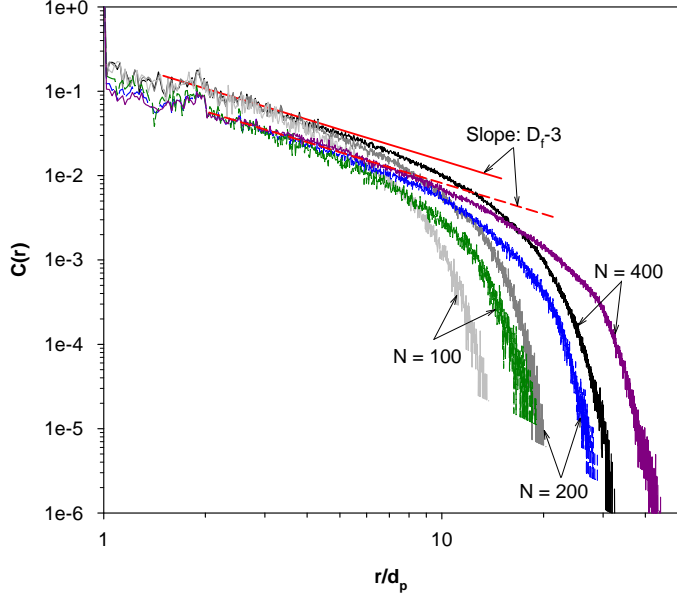


Fig. 3 Autocorrelation functions for fractal aggregates generated using the following parameters:  $a = 15$  nm,  $D_f = 1.78$ ,  $k_f = 1.3$  or  $2.3$ . The black and grey curves are for  $k_f = 2.3$ . The colored curves are for  $k_f = 1.3$

### Generalized Multi-sphere Mie-Solution

In this study GMM was used to calculate the orientation-averaged radiative properties of the numerically generated fractal aggregates. GMM is numerically exact and much more efficient than many other numerical techniques based on an explicit solution of the Maxwell equations. GMM was developed by Xu [14,15] based on the framework of the Mie theory for a single sphere and the addition theorems for spherical vector wave functions. GMM provides a rigorous and complete solution to non-overlapping multisphere light scattering problems and can be readily applied to fractal aggregates [5,10]. The key steps involved in the development of GMM include: (a) expansion of the scattered, internal, and incident electromagnetic fields in terms of vector spherical functions, (b) formation of a linear equation system through the boundary condition at each primary particle in the aggregate, (c) transformation of the waves scattered by an individual primary particle into the incident waves of the other particles in the aggregate through the addition theorems for vector spherical functions, and (d) solution of the linear system of interactive coefficients. The absorption and scattering cross sections and the four scattering matrix coefficients are analytically given by Xu [14,15]. GMM rigorously accounts for

the multiple scattering within the aggregate. However, GMM is very computationally demanding and memory intensive for large aggregates containing several hundred primary particles, especially when the size parameter of primary particle is relatively large.

### RDG theory for fractal aggregates

The RDG theory applied to monodisperse fractal aggregates has been described in detail in the literature, e.g. [7]. Only the main results are summarized here. RDG theory is based on the assumption that primary particles are in the Rayleigh regime, where the absorption and scattering cross-sections are given as

$$C_a^p = \frac{4\pi x_p^3 E(m)}{k^2}, C_s^p = \frac{8\pi x_p^6 F(m)}{3k^2}, C_{vv}^p = \frac{x_p^6 F(m)}{k^2} \quad (5)$$

where superscript  $p$  denotes primary particle,  $m$  is the refractive index,  $E(m) = \text{Im}((m^2-1)/(m^2+2))$ ,  $F(m) = |(m^2-1)/(m^2+2)|^2$ , and  $k$  is the wave number ( $2\pi/\lambda$ ). The differential scattering cross sections of an aggregate of size  $N$  for polarized light are given as

$$C_{vv}^a(\theta) = C_{hh}^a(\theta) / \cos^2 \theta = N^2 C_{vv}^p f(qR_g) \quad (6)$$

where superscript  $a$  stands for aggregate, subscripts  $vv$  and  $hh$  stand for vertical-vertical and horizontal-horizontal (where the first symbol is for the incident light and the second is for the scattered light),  $q = 2k\sin(\theta/2)$  is the modulus of scattering vector and  $f(qR_g)$  is the so-called aggregate form factor, which can be written in two different expressions in the small angle Guinier regime and in the large angle power-law regime, e.g. [7], as

$$f(qR_g) = \exp(-(qR_g)^2 / 3), \text{ Guinier regime} \quad (7)$$

$$f(qR_g) = (qR_g)^{-D_f}, \text{ Power-law regime} \quad (8)$$

The boundary between the Guinier and the power-law regimes is taken as  $qR_g = (1.5D_f)^{0.5}$  [7]. The total scattering cross-section is given as [7]

$$C_{sca}^a = N^2 C_{sca}^p g(kR_g, D_f) \quad (9)$$

where the aggregate total scattering factor takes the following expression [7]

$$g(kR_g, D_f) = 1 - 2(kR_g)^2 / 3, \text{ if } \beta = 3D_f / (8k^2 R_g^2) \geq 1 \quad (10)$$

$$g(kR_g, D_f) = \frac{\beta}{2} (3 - 3\beta + 2\beta^2) - \frac{(kR_g \beta)^2}{3} (3 - 4\beta + 3\beta^2) + (2kR_g)^{-D_f} \left[ \frac{3}{2 - D_f} - \frac{12}{(6 - D_f)(4 - D_f)} - 3\beta^{1-D_f/2} \left( \frac{1}{2 - D_f} - \frac{2\beta}{4 - D_f} + \frac{2\beta^2}{6 - D_f} \right) \right], \text{ if } \beta < 1 \quad (11)$$

The effect of aggregation on aggregate absorption is completely neglected so that the absorption cross-section in RDG is simply calculated as

$$C_{abs}^a = N C_{abs}^p \quad (12)$$

It is expected from Eqs. (6) and (8) that the non-dimensional vertical-vertical differential scattering cross-section from the RDG theory can be written as

$$\frac{C_{vv}^a}{NC_{vv}^p} = N \exp(-(qR_g)^2 / 3) = k_f (qa)^{-D_f} \quad (13)$$

In deriving the second part of Eq. (13) the radius of gyration from Eq. (1) is substituted into the first part. Eq. (13) can be used to recover the fractal dimension  $D_f$  and prefactor  $k_f$  once the aggregate differential scattering cross-section is available either from experimental measurement or numerical calculations. Eq. (13) indicates that

$$D_f = -\frac{\log((C_{vv}^a / NC_{vv}^p) / k_f)}{\log(qa)} \quad (14)$$

i.e.,  $D_f$  is the slope of the non-dimensional differential scattering cross-section vs.  $qa$  in the power-law regime on a log-log scale.  $k_f$  is simply the value of the non-dimensional differential scattering cross-section at  $qa = 1$  (or equivalently  $qd_p = 2$ ). It should be pointed out that extrapolation in general is required since  $qa = 1$  is often not reached.

## RESULTS AND DISCUSSION

Numerical calculations were conducted for 266 nm wavelength to achieve a relatively large primary particle size parameter of  $x_p$  ( $\pi d_p / \lambda$ ) = 0.354 so that the power-law regime can be reached comfortably for a relatively small aggregate size of 50. However, it is noticed that this value is still quite small and is considered on the borderline for the RDG approximation to be valid, which is normally taken as  $x_p < \approx 0.3$ . The refractive index of soot was assumed to be  $m = 1.6 + 0.6i$ . Orientation averaging was achieved numerically in the GMM calculations by dividing each Euler angle into at least 15 equal-intervals, giving the total orientations more than 3375. Such level of orientation averaging is considered adequate based on previous studies [16], i.e., further division of the three Euler angles would not significantly affect the orientation averaged results. It is noticed that this study employed far more orientations in the orientation averaging than the study of Brasil et al. [6], where only 16 orientations were considered. All the GMM results presented below were also averaged over at least 10 aggregate realizations of identical parameters ( $a$ ,  $N$ ,  $D_f$ ,  $k_f$ ). Such level of realization averaging is considered adequate based on our recent study [11].

### Differential scattering cross-section $C_{vv}^a$

The non-dimensional differential scattering cross sections  $C_{vv}^a$ , normalized by  $NC_{vv}^p$  for  $k_f = 1.3$  are compared with those from RDG in Fig. 4. The vertical dotted lines mark the boundary between the Guinier and the power-law regimes. The difference between the GMM and RDG results is small for  $N = 50$  and 100, Figs. 4(a) and 4(b), but becomes more pronounced for  $N = 200$  and 400, Figs. 4(c) and 4(d). It is noticed that the RDG results recover the morphological fractal dimension and prefactor, as expected.

The fractal parameters ( $D_f$  and  $k_f$ ) recovered from the GMM results shown in Fig. 4 are compared with those of morphological ones in Table 1. In this case, where the specified

prefactor is  $k_f = 1.3$ , the inferred fractal dimensions from the predicted light scattering properties of different aggregate sizes are only slightly higher than the specified value of 1.78 and there is no clear trend for the variation of  $D_{f,LS}$  with aggregate size. However, it is evident that  $k_{f,LS}$  decreases with increasing the aggregate size. This is attributed to the fact that the GMM differential scattering cross section becomes increasingly lower than the RDG one in the power-law regime as  $N$  increases (recall that  $k_{f,LS}$  is the value of  $C_{vv}^a / (NC_{vv}^p)$  at  $qd_p = 2$ ). As pointed out earlier, RDG neglects multiple scattering among primary particles within aggregate while GMM fully account for multiple scattering. Therefore, the deviation of the GMM results from the RDG ones can be largely attributed to the effect of multiple scattering. It is well known that multiple scattering yields less scattering as a result of interference [12]. This explains why GMM results are consistently less than those of RDG in the entire range of  $qd_p$ .

Results shown in Table 1 suggest that in this case ( $k_{f,M} = 1.3$ ) the calculated light scattering property can be used to infer the fractal dimension. However, the inferred prefactor is likely to be lower than the morphological value.

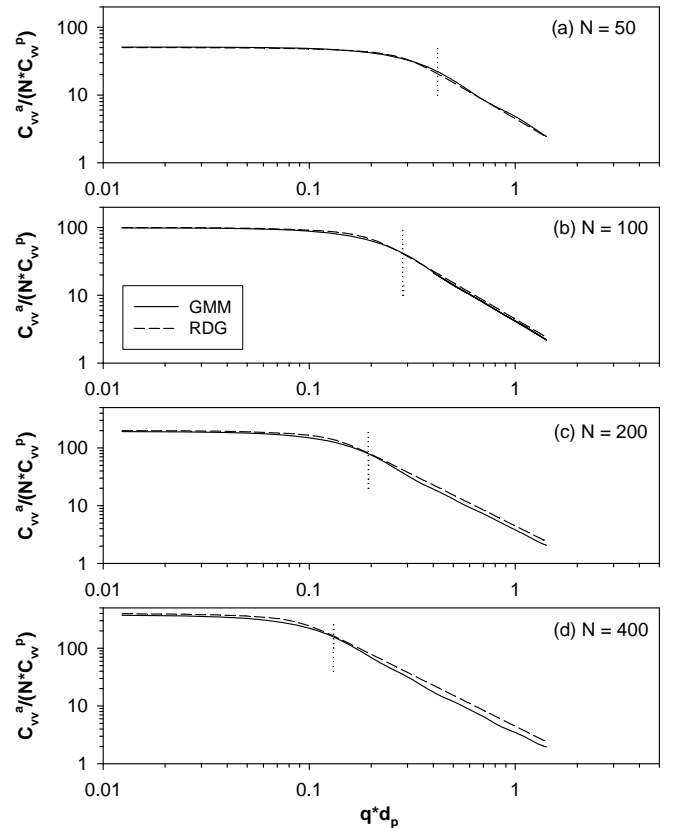


Fig. 4 Comparison of the non-dimensional differential scattering cross-sections  $C_{vv}^a$  calculated by GMM and RDG for  $D_f = 1.78$ ,  $k_f = 1.3$ ,  $a = 15$  nm, and different aggregate size  $N$

Table 1 Comparison of fractal dimension and prefactor recovered from the GMM non-dimensional differential scattering cross section and the corresponding morphological values for  $k_f = 1.3$ .

$N$	$k_{f,LS}$	$D_{f,LS}$	$k_{f,M}$	$D_{f,M}$
50	1.346	1.785	1.3	1.78
100	1.196	1.791	1.3	1.78
200	1.105	1.782	1.3	1.78
400	1.019	1.785	1.3	1.78

The non-dimensional vertical-vertical differential scattering cross sections calculated by GMM for  $k_f = 2.3$  are compared with those from RDG in Fig. 5. Again, the vertical dotted lines mark the boundary between the Guinier and the power-law regimes. Compared to the results shown in Fig. 4, two observations can be readily made. First, the slope of GMM results in the power-law regime is significantly steeper than that of RDG for all the aggregate sizes considered. Secondly, the GMM differential scattering cross sections are more significantly lower than those of RDG. It is therefore expected that the recovered fractal dimension and prefactor based on the GMM results can be quite different from the morphological values. Table 2 compares the fractal dimension and prefactor inferred from the GMM scattering results and those of the morphological ones, which are the same as those inferred from the RDG results. The fractal dimensions inferred from the GMM scattering property,  $D_{f,LS}$ , are significantly larger than the morphological one. In addition,  $D_{f,LS}$  decreases with increasing the aggregate size  $N$ , reflecting the fact that the slope of the non-dimensional  $C_{vv}^a$  in the power-law regime becomes more gentle as  $N$  increases, Fig. 5. On the other hand, the GMM scattering property inferred prefactor,  $k_{f,LS}$ , are much smaller than the morphological value of 2.3. Both the steeper slope of the GMM results and the departure of the GMM results from those of RDG contribute to the smallness of  $k_{f,LS}$ . The former is more significant at small  $N$  (e.g., 50), while the latter is more pronounced at large  $N$  (e.g., 400). As a result, the inferred prefactor is more or less independent of aggregate size  $N$ , Table 2. It is noticed that fractal prefactors less than unity have not been reported in previous studies.

The results shown in Figs. 4 and 5 and Tables 1 and 2 illustrate a fundamental drawback of using light scattering property to infer the fractal parameters of fractal aggregates: effects of multiple scattering are inherently present in either experimentally measured or numerically calculated (using sufficiently accurate methods) light scattering properties while as the current theory behind this practice is based on the RDG approximation, which neglects multiple scattering. Consequently, it is not surprising to find out that the inferred fractal dimension and prefactor from the calculated light scattering properties are in general different from the morphological values, as shown above and in the study of Brasil et al. [6]. Therefore, multiple scattering is the cause responsible for the discrepancy between the light scattering inferred fractal parameters and the morphological ones in the

present context. Besides multiple scattering, the potential effect of primary particle bridging discussed by Brasil et al. [6] and polydispersity of aggregates could also affect the fractal parameters derived from experimentally measured light scattering properties of soot.

Table 2 Comparison of fractal dimension and prefactor recovered from the GMM non-dimensional differential scattering cross section and the corresponding morphological values for  $k_f = 2.3$ .

$N$	$k_{f,LS}$	$D_{f,LS}$	$k_{f,M}$	$D_{f,M}$
50	0.727	2.812	2.3	1.78
100	0.705	2.565	2.3	1.78
200	0.714	2.373	2.3	1.78
400	0.729	2.232	2.3	1.78

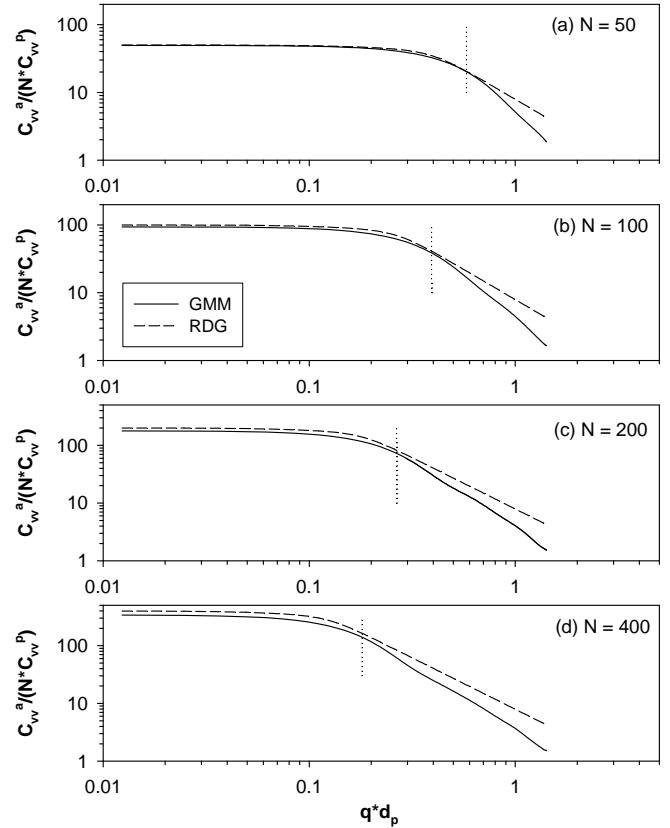


Fig. 5 Comparison of non-dimensional differential scattering cross-sections calculated by GMM and RDG for  $D_f = 1.78$ ,  $k_f = 2.3$ , and different aggregate size  $N$

A closer look at Figs. 4 and 5 indicate that the prefactor  $k_f$  affects the RDG and GMM vertical-vertical differential scattering cross sections. The effect of  $k_f$  on  $C_{vv}^a$  can be illustrated by plotting the aggregate form factor given in Eqs. (7) and (8). Fig. 6 shows the aggregate form factor for different values of  $k_f$  and aggregate size  $N$ . It is evident that for a given aggregate size the form factor is larger for a larger  $k_f$  over the

entire range of  $qd_p$ . This result can be explained as follows. A larger value of  $k_f$  means a more compact aggregate. Therefore, the scattered light by primary particles within this aggregate are more likely to be in-phase, leading to higher scattering cross section.

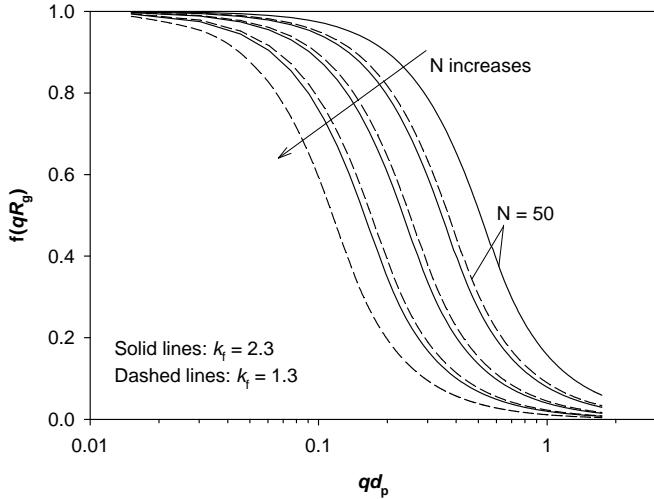


Fig. 6 Aggregate form factors for different  $k_f$  and aggregate size  $N$  (50, 100, 200, and 400) with  $a = 15$  nm,  $D_f = 1.78$

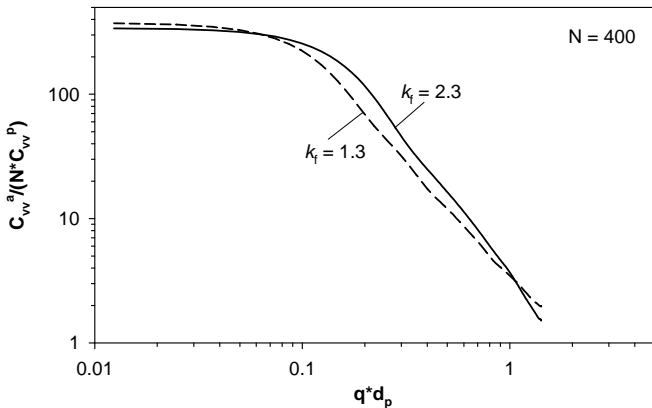


Fig. 7 Comparison of non-dimensional differential scattering cross section for  $k_f = 1.3$  and  $2.3$  and  $N = 400$

The effect of  $k_f$  on the GMM results is less straightforward due to two competing influences of increasing  $k_f$ , i.e., the increase in  $k_f$  results in a more compact structure, which enhances scattering on one hand as the scattered light by primary particles are more likely to be in-phase and also weakens scattering on the other hand through multiple scattering. Fig. 7 illustrates these two processes through the comparison of non-dimensional vertical-vertical differential scattering cross section for  $N = 400$ . It is seen that in the small angle forward directions (small values of  $qd_p$ ) the differential scattering cross sections for  $k_f = 2.3$  are actually lower than those for  $k_f = 1.3$ , while as the RDG results are just the opposite. At larger scattering angles, the differential scattering cross sections for  $k_f = 2.3$  become higher, in agreement with the

trend of the RDG approximation. At the backward directions, the differential scattering cross sections for  $k_f = 2.3$  become smaller again due to a steeper slope of the differential scattering cross section.

### Absorption and total scattering cross sections

The non-dimensional aggregate absorption cross sections for different prefactors are compared in Fig. 8. Since the effect of aggregation on aggregate absorption is completely neglected in RDG, the RDG non-dimensional aggregate absorption cross section remains unity regardless the value of  $k_f$  or  $N$ . However, the prefactor does affect the aggregate absorption cross section predicted by GMM in such a way that a higher  $k_f$  yields lower absorption cross sections. This influence of the prefactor may be explained in terms of the shielding effect, which is expected to be stronger for a more compact aggregate associated with a higher  $k_f$ . The decreasing absorption ability of aggregate with increasing size can also be explained by the shielding effect. It is noticed that the GMM absorption cross sections can become smaller than those of RDG for sufficiently large aggregates.

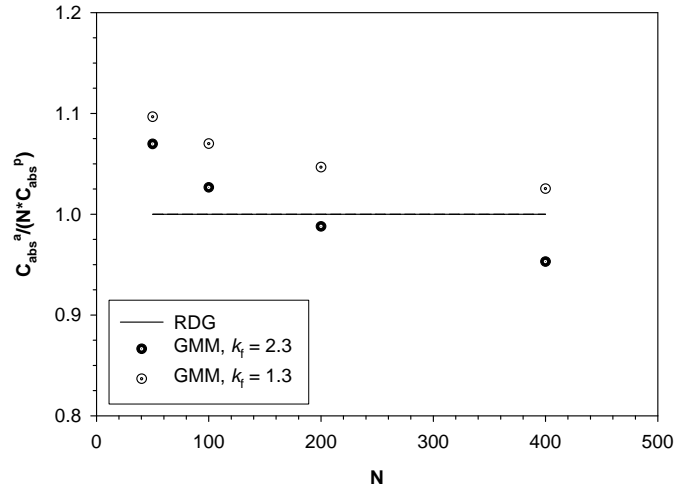


Fig. 8 Non-dimensional aggregate absorption cross sections from RDG and GMM and different prefactors. The following parameters are fixed:  $a = 15$  nm,  $D_f = 1.78$

The non-dimensional aggregate total scattering cross sections from RDG and GMM and different values of  $k_f$  are compared in Fig. 9. It is first noticed that a higher  $k_f$  gives rise to higher total scattering cross sections due to the likelihood of being in-phase for the scattered light by primary particles for a more compact structure. This trend is just opposite to the effect of  $k_f$  on the aggregate absorption cross section shown in Fig. 8. For  $k_f = 2.3$ , the total scattering cross sections from GMM are increasingly smaller than those of RDG as  $N$  increases, which is consistent with the differential scattering cross sections shown in Fig. 5. For  $k_f = 1.3$ , the discrepancies between the RDG and GMM results are fairly small, again consistent with the relatively small differences between the RDG and GMM differential scattering cross sections shown in Fig. 4. It is noticed that for  $N = 50$  and  $100$  the GMM total scattering cross

sections are actually greater than those of RDG. For larger aggregates, i.e.,  $N = 200$  and  $400$ , the results of GMM are smaller. The difference between the RDG and GMM total scattering cross sections shown in Fig. 9 can be attributed to the effect of multiple scattering and Fig. 9 is another way, in addition to the results shown in Figs. 4 and 5, to quantify such effect.

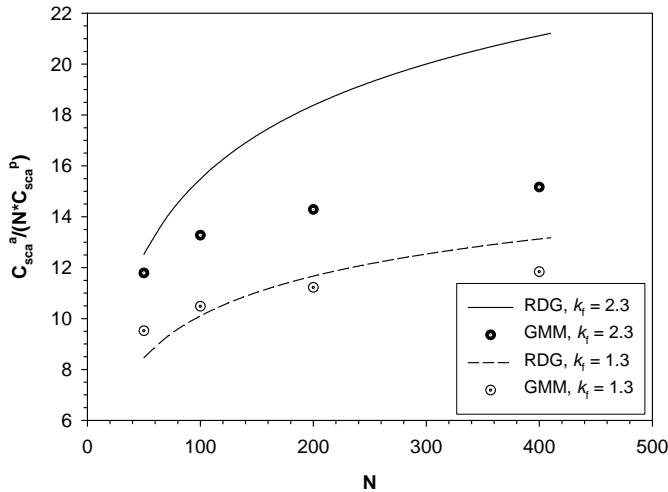


Fig. 9 Non-dimensional aggregate total scattering cross sections from RDG and GMM and different prefactors. The following parameters are fixed:  $a = 15$  nm,  $D_f = 1.78$

## CONCLUSIONS

The effects of prefactor on the optical properties of fractal soot aggregates were investigated by employing the generalized Mie-solution method for numerically generated fractal aggregates. The methodology used in this work is superior to previous studies in terms of the accuracy of the numerical method for calculating the optical properties and the consistency of fractal parameters from one aggregate realization to another of the same size.

Numerical results show that the prefactor affects both the absorption and scattering properties of numerically generated fractal soot aggregates. A smaller prefactor gives rise to larger absorption cross sections but smaller total scattering cross sections. The effect of prefactor on the vertical-vertical differential cross section is dependent on the scattering angle. In the forward small angle regime, the differential scattering cross section is smaller for a larger prefactor. However, it becomes larger for intermediate scattering angles.

Large differences were found between the RDG and GMM results, suggesting the effect of multiple scattering is significant. For a relatively open aggregate structure with a prefactor of 1.3, the inferred fractal dimensions from the GMM scattering results are in good agreement with the morphological value; however, the inferred prefactor is somewhat lower. For a more compact aggregate structure with a prefactor of 2.3, the recovered fractal dimension from the GMM results is much

higher than the morphological value while as the recovered prefactor is much lower than the morphological one.

The discrepancy between the inferred fractal parameters based on either numerically calculated or experimentally measured scattering properties, which inherently contain the effects of multiple scattering, and the morphological ones is attributed to multiple scattering. The current theory behind this practice neglects the role of multiple scattering. Therefore, the fractal parameters of soot inferred from light scattering experiments may not be as reliable as previously thought. Further studies are required to investigate the effect of polydispersity of soot aggregates and how to properly recover fractal parameters from light scattering experiments in the presence of multiple scattering.

## ACKNOWLEDGMENTS

We would like to thank Dr. Y.-L. Xu for making his GMM computer codes available. Financial support was provided in part by the Government of Canada's PERD Program through Projects C23.006 and C11.003.

## REFERENCES

1. Dalzell, W. H., Williams, G. C., and Hottel, H. C., 1970, "A light-scattering method for soot concentration measurements," *Combust. Flame* **14**, pp. 161-170.
2. Köylü, Ü. Ö., and Faeth, G. M., 1993, "Radiative properties of flame-generated soot," *J. Heat Transfer* **115**, 1993, pp. 409-417.
3. Farias, T. L., Carvalho, M. G., Köylü, Ü. Ö., and Faeth, G. M., 1995, "Computational evaluation of approximate Rayleigh-Debye-Gans/fractal-aggregate theory for the absorption and scattering properties of soot," *J. Heat Transfer* **117**, pp. 152-159.
4. Farias, T. L., Köylü, Ü. Ö., and Carvalho, M. G., 1996, "Range of validity of the Rayleigh-Debye-Gans theory for optics of fractal aggregates," *Applied Optics* **35**, No. 33, pp. 6560-6567.
5. Liu, F., Snelling, D. R., 2008, "Evaluation of the accuracy of the RDG approximation for the absorption and scattering properties of fractal aggregates of flame-generated soot," AIAA-2008-4362.
6. Brasil, A. M., Farias, T. L., and Carvalho, M. G., 2000, "Evaluation of the fractal properties of cluster-cluster aggregates," *Aerosol Sci. Tech.* **33**, pp. 440-454.
7. Köylü, Ü. Ö., and Faeth, G. M., 1994, "Optical properties of overfire soot in buoyant turbulent diffusion flames at long residence times," *J. Heat Transfer* **116**, pp. 152-159.
8. Forrest, S. R., and Witten Jr., T. A., 1979, "Long-range correlations in smoke-particle aggregates," *J. Phys. A: Math. Gen* **12**, pp. L109-L117.
9. Filippov, A. V., Zurita, M., and Rosner, D. E., 2000, "Fractal-like aggregates: relation between morphology and physical properties," *J. Colloid Interface Sci.* **229**, pp. 261-273.

10. Van-Hulle, P., Weill, M.-E., Talbaut, M., and Coppalle, A., 2002, "Comparison of numerical studies characterizing optical properties of soot aggregates for improved EXSCA measurements," *Part. Part. Syst. Charact.* **19**, pp. 47-57.
11. Liu, F., and Smallwood, G. J., 2009, "Radiative properties of numerically generated fractal soot aggregates: the importance of configuration averaging," HT2009-88224, Proceedings of 2009 ASME Summer Heat Transfer Conference, July 19-23, 2009, San Francisco, California, USA.
12. Sorensen, C. M., 2001, "Light scattering by fractal aggregates: a review," *Aerosol Sci. Tech.* **35**, pp. 648-687.
13. Hasmy, A., Foret, M., Pelous, J., and Jullien, R., 1993, "Small-angle neutron-scattering investigation of short-range correlations in fractal aerosols: simulations and experiments," *Phys. Rev. B.* **48**, pp. 9345-9353.
14. Xu, Y.-L., 1995, "Electromagnetic scattering by an aggregate of spheres," *Applied Optics* **34**, pp. 4573-4588.
15. Xu, Y.-L., 1997, "Electromagnetic scattering by an aggregate of spheres: far field," *Applied Optics* **36**, pp. 9496-9508.
16. Riefler, N., di Stasio, S., and Wriedt, T., 2004, "Structural analysis of clusters using configurational and orientational averaging in light scattering analysis," *JQSRT* **89**, pp. 323-342.
17. Farias, T. L., Carvalho, M. G., Köylü, Ü. Ö., and Faeth, G. M., 1995, "Computational evaluation of approximate Rayleigh-Debye-Gans/fractal-aggregate theory for the absorption and scattering properties of soot," *J. Heat Transfer* **117**, pp. 152-159.